

Measurements of J/ψ Decays into $2(\pi^+\pi^-)\eta$ and $3(\pi^+\pi^-)\eta$

M. Ablikim¹, J. Z. Bai¹, Y. Ban¹¹, J. G. Bian¹, X. Cai¹, J. F. Chang¹,
H. F. Chen¹⁷, H. S. Chen¹, H. X. Chen¹, J. C. Chen¹, Jin Chen¹, Jun Chen⁷,
M. L. Chen¹, Y. B. Chen¹, S. P. Chi², Y. P. Chu¹, X. Z. Cui¹, H. L. Dai¹,
Y. S. Dai¹⁹, Z. Y. Deng¹, L. Y. Dong^{1a}, Q. F. Dong¹⁵, S. X. Du¹, Z. Z. Du¹,
J. Fang¹, S. S. Fang², C. D. Fu¹, H. Y. Fu¹, C. S. Gao¹, Y. N. Gao¹⁵,
M. Y. Gong¹, W. X. Gong¹, S. D. Gu¹, Y. N. Guo¹, Y. Q. Guo¹, Z. J. Guo¹⁶,
F. A. Harris¹⁶, K. L. He¹, M. He¹², X. He¹, Y. K. Heng¹, H. M. Hu¹, T. Hu¹,
G. S. Huang^{1b}, X. P. Huang¹, X. T. Huang¹², X. B. Ji¹, C. H. Jiang¹,
X. S. Jiang¹, D. P. Jin¹, S. Jin¹, Y. Jin¹, Yi Jin¹, Y. F. Lai¹, F. Li¹, G. Li²,
H. H. Li¹, J. Li¹, J. C. Li¹, Q. J. Li¹, R. Y. Li¹, S. M. Li¹, W. D. Li¹,
W. G. Li¹, X. L. Li⁸, X. Q. Li¹⁰, Y. L. Li⁴, Y. F. Liang¹⁴, H. B. Liao⁶,
C. X. Liu¹, F. Liu⁶, Fang Liu¹⁷, H. H. Liu¹, H. M. Liu¹, J. Liu¹¹, J. B. Liu¹,
J. P. Liu¹⁸, R. G. Liu¹, Z. A. Liu¹, Z. X. Liu¹, F. Lu¹, G. R. Lu⁵, H. J. Lu¹⁷,
J. G. Lu¹, C. L. Luo⁹, L. X. Luo⁴, X. L. Luo¹, F. C. Ma⁸, H. L. Ma¹,
J. M. Ma¹, L. L. Ma¹, Q. M. Ma¹, X. B. Ma⁵, X. Y. Ma¹, Z. P. Mao¹,
X. H. Mo¹, J. Nie¹, Z. D. Nie¹, S. L. Olsen¹⁶, H. P. Peng¹⁷, N. D. Qi¹,
C. D. Qian¹³, H. Qin⁹, J. F. Qiu¹, Z. Y. Ren¹, G. Rong¹, L. Y. Shan¹,
L. Shang¹, D. L. Shen¹, X. Y. Shen¹, H. Y. Sheng¹, F. Shi¹, X. Shi^{1c},
H. S. Sun¹, J. F. Sun¹, S. S. Sun¹, Y. Z. Sun¹, Z. J. Sun¹, X. Tang¹,
N. Tao¹⁷, Y. R. Tian¹⁵, G. L. Tong¹, G. S. Varner¹⁶, D. Y. Wang¹,
J. Z. Wang¹, K. Wang¹⁷, L. Wang¹, L. S. Wang¹, M. Wang¹, P. Wang¹,
P. L. Wang¹, S. Z. Wang¹, W. F. Wang^{1d}, Y. F. Wang¹, Z. Wang¹,
Z. Y. Wang¹, Zhe Wang¹, Zheng Wang², C. L. Wei¹, D. H. Wei¹, N. Wu¹,
Y. M. Wu¹, X. M. Xia¹, X. X. Xie¹, B. Xin^{8b}, G. F. Xu¹, H. Xu¹, S. T. Xue¹,
M. L. Yan¹⁷, F. Yang¹⁰, H. X. Yang¹, J. Yang¹⁷, Y. X. Yang³, M. Ye¹,
M. H. Ye², Y. X. Ye¹⁷, L. H. Yi⁷, Z. Y. Yi¹, C. S. Yu¹, G. W. Yu¹,
C. Z. Yuan¹, J. M. Yuan¹, Y. Yuan¹, S. L. Zang¹, Y. Zeng⁷, Yu Zeng¹,
B. X. Zhang¹, B. Y. Zhang¹, C. C. Zhang¹, D. H. Zhang¹, H. Y. Zhang¹,
J. Zhang¹, J. W. Zhang¹, J. Y. Zhang¹, Q. J. Zhang¹, S. Q. Zhang¹,
X. M. Zhang¹, X. Y. Zhang¹², Y. Y. Zhang¹, Yiyun Zhang¹⁴, Z. P. Zhang¹⁷,
Z. Q. Zhang⁵, D. X. Zhao¹, J. B. Zhao¹, J. W. Zhao¹, M. G. Zhao¹⁰,
P. P. Zhao¹, W. R. Zhao¹, X. J. Zhao¹, Y. B. Zhao¹, Z. G. Zhao^{1e},
H. Q. Zheng¹¹, J. P. Zheng¹, L. S. Zheng¹, Z. P. Zheng¹, X. C. Zhong¹,
B. Q. Zhou¹, G. M. Zhou¹, L. Zhou¹, N. F. Zhou¹, K. J. Zhu¹, Q. M. Zhu¹,
Y. C. Zhu¹, Y. S. Zhu¹, Yingchun Zhu^{1f}, Z. A. Zhu¹, B. A. Zhuang¹,
X. A. Zhuang¹, B. S. Zou¹
(BES Collaboration)

¹*Institute of High Energy Physics, Beijing 100049, People's Republic of*

China

²China Center for Advanced Science and Technology, Beijing 100080,
People's Republic of China

³Guangxi Normal University, Guilin 541004, People's Republic of China

⁴Guangxi University, Nanning 530004, People's Republic of China

⁵Henan Normal University, Xinxiang 453002, People's Republic of China

⁶Huazhong Normal University, Wuhan 430079, People's Republic of China

⁷Hunan University, Changsha 410082, People's Republic of China

⁸Liaoning University, Shenyang 110036, People's Republic of China

⁹Nanjing Normal University, Nanjing 210097, People's Republic of China

¹⁰Nankai University, Tianjin 300071, People's Republic of China

¹¹Peking University, Beijing 100871, People's Republic of China

¹²Shandong University, Jinan 250100, People's Republic of China

¹³Shanghai Jiaotong University, Shanghai 200030, People's Republic of
China

¹⁴Sichuan University, Chengdu 610064, People's Republic of China

¹⁵Tsinghua University, Beijing 100084, People's Republic of China

¹⁶University of Hawaii, Honolulu, Hawaii 96822, USA

¹⁷University of Science and Technology of China, Hefei 230026, People's
Republic of China

¹⁸Wuhan University, Wuhan 430072, People's Republic of China

¹⁹Zhejiang University, Hangzhou 310028, People's Republic of China

^a Current address: Iowa State University, Ames, Iowa 50011-3160, USA.

^b Current address: Purdue University, West Lafayette, Indiana 47907, USA.

^c Current address: Cornell University, Ithaca, New York 14853, USA.

^d Current address: Laboratoire de l'Accélérateur Linéaire, F-91898 Orsay,
France.

^e Current address: University of Michigan, Ann Arbor, Michigan 48109, USA.

^f Current address: DESY, D-22607, Hamburg, Germany.

Abstract

Based on a sample of 5.8×10^7 J/ψ events taken with the BESII detector, the branching fractions of $J/\psi \rightarrow 2(\pi^+\pi^-)\eta$ and $J/\psi \rightarrow 3(\pi^+\pi^-)\eta$ are measured for the first time to be $(2.26 \pm 0.08 \pm 0.27) \times 10^{-3}$ and $(7.24 \pm 0.96 \pm 1.11) \times 10^{-4}$, respectively.

PACS: 13.25.Gv, 14.40.Gx, 13.40.Hq

1 Introduction

More than one hundred exclusive decay modes of the J/ψ have been reported since its discovery at Brookhaven [1] and SLAC [2] in 1974. According to Ref. [3], direct hadronic, electromagnetic and radiative decays represent roughly 65%, 14%, and 7% of the total J/ψ decay rate, respectively. Up to now, only about half of all hadronic decays, 34.8%, have been measured in exclusive reactions. The sample of 58 million J/ψ events, taken at BESII, provides a chance to measure some of the missing hadronic decays. In this analysis, we report the first measurements of $J/\psi \rightarrow 2(\pi^+\pi^-)\eta$ and $J/\psi \rightarrow 3(\pi^+\pi^-)\eta$.

The upgraded Beijing Spectrometer (BESII) detector located at the Beijing Electron-Positron Collider (BEPC) is a large solid-angle magnetic spectrometer which is described in detail in Ref. [4]. The momentum of the charged particle is determined by a 40-layer cylindrical main drift chamber (MDC) which has a momentum resolution of $\sigma_p/p = 1.78\% \sqrt{1 + p^2}$ (p in GeV/c). Particle identification is accomplished by specific ionization (dE/dx) measurements in the drift chamber and time-of-flight (TOF) information in a barrel-like array of 48 scintillation counters. The dE/dx resolution is $\sigma_{dE/dx} = 8.0\%$; the TOF resolution for Bhabha events is $\sigma_{TOF} = 180$ ps. Radially outside of the time-of-flight counters is a 12-radiation-length barrel shower counter (BSC) comprised of gas tubes interleaved with lead sheets. The BSC measures the energy and direction of photons with resolutions of $\sigma_E/E \simeq 21\% \sqrt{E}$ (E in GeV), $\sigma_\phi = 7.9$ mrad, and $\sigma_z = 2.3$ cm. The iron flux return of the magnet is instrumented with three double layers of counters that are used to identify muons.

A GEANT3 based Monte Carlo package (SIMBES) with detailed consideration of the detector performance is used. The consistency between data and Monte Carlo has been carefully checked in many high purity physics channels, and the agreement is reasonable.

2 Analysis of $J/\psi \rightarrow 2(\pi^+\pi^-)\eta$

This decay is observed in the topology $\pi^+\pi^-\pi^-\pi^-\gamma\gamma$. Events with four charged tracks and at least two isolated photons are selected. The selection criteria for charged tracks and photons are described in detail in Ref. [5]. Each charged track must be well fitted to a helix, originating from the interaction region of $R_{xy} < 0.02$ m and $|z| < 0.2$ m, and have a polar angle, θ , in the range $|\cos\theta| < 0.8$.

Isolated photons are those that have energy deposited in the BSC greater

than 60 MeV, the angle between the direction at the first layer of the BSC and the developing direction of the cluster less than 30° , and the angle between photons and any charged tracks larger than 10° . To eliminate tracks from γ conversions, the minimum angle between any two oppositely-charged tracks is required to be greater than 10° .

A 4C kinematic fit is performed under the hypothesis $\pi^+\pi^-\pi^+\pi^-\gamma\gamma$, and the chi-squared, $\chi_{\pi^+\pi^-\pi^+\pi^-\gamma\gamma}^2$, is required to be less than 15. $\chi_{\pi^+\pi^-\pi^+\pi^-\gamma\gamma}^2$ is also required to be less than the chi-squares for the $K^+K^-\pi^+\pi^-\gamma\gamma$ and $\pi^+\pi^-\pi^+\pi^-\gamma\gamma\gamma$ hypotheses.

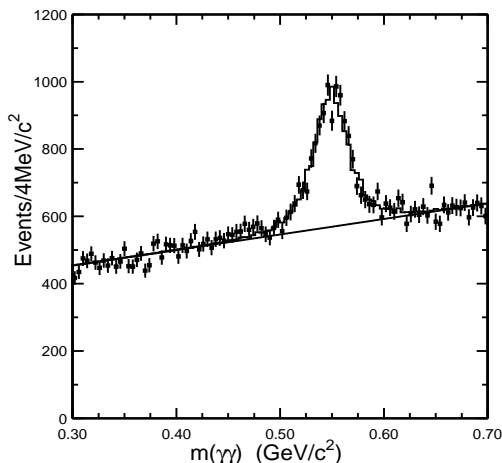


Fig. 1. The distribution of $m_{\gamma\gamma}$ for candidate $J/\psi \rightarrow \eta 2(\pi^+\pi^-)$ events. Dots with error bars are data, the histogram is the shape of the η from Monte Carlo simulation, and the curve is background.

After the above selection, the $m_{\gamma\gamma}$ distribution is shown in Fig. 1, where a clear η signal is observed. Monte Carlo simulation is used to estimate the background, and backgrounds from simulated channels are listed in Table 1, where N_{sel}^{MC} is the number of events after event selection and N^{norm} is the background normalized to 58 million J/ψ events. The sum of background events is 18 events, which can be ignored. Another possible background channel is from $J/\psi \rightarrow \gamma\eta 2(\pi^+\pi^-)$. No obvious η signal is seen in the $m_{\gamma\gamma}$ distribution from $J/\psi \rightarrow \gamma\eta 2(\pi^+\pi^-)$, as shown in Fig. 2(a). Therefore the background from this channel can also be ignored.

Background from events with a K_S^0 in the final state are estimated from η sidebands. Fig. 2(b) shows the mass distribution of all $\pi^+\pi^-$ pairs for events with $m_{\gamma\gamma}$ in the η region ($|m_{\gamma\gamma} - 0.55| < 0.05$ GeV/ c^2), and the shaded

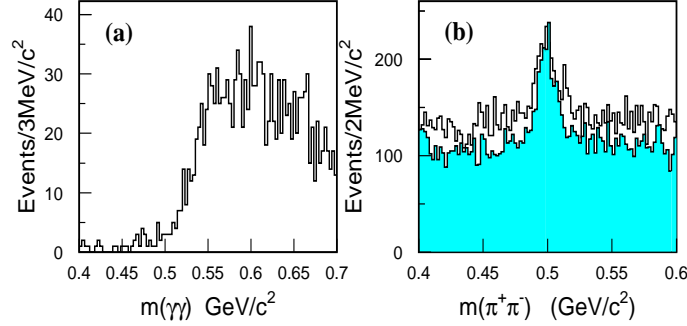


Fig. 2. (a) Distribution of $m_{\gamma\gamma}$ from Monte Carlo simulation of $J/\psi \rightarrow \gamma 2(\pi^+\pi^-)\eta$. (b) Distribution of $m_{\pi^+\pi^-}$ from the η signal region (blank histogram) and η sidebands (shaded histogram) for $J/\psi \rightarrow \gamma\gamma 2(\pi^+\pi^-)$ events.

Table 1

Background estimates for the $J/\psi \rightarrow \eta 2(\pi^+\pi^-)$ case. N_{sel}^{MC} are the number of events passing selection criteria; N^{norm} is the background normalized to 58 million J/ψ events.

Channel	MC sample	N_{sel}^{MC}	N^{norm}
$J/\psi \rightarrow \phi\eta$	40,000	0	0
$J/\psi \rightarrow \rho\eta$	40,000	0	0
$J/\psi \rightarrow \gamma\eta\pi^+\pi^-$	70,000	2	3
$J/\psi \rightarrow \omega\eta(\eta \rightarrow \gamma\gamma)$	40,000	11	8
$J/\psi \rightarrow \omega\eta'(\eta' \rightarrow \pi^+\pi^-\eta)$	100,000	135	2
$J/\psi \rightarrow \phi\eta'(\eta' \rightarrow \pi^+\pi^-\eta)$	40,000	2	0
$J/\psi \rightarrow \gamma\eta'(\eta' \rightarrow \pi^+\pi^-\eta)$	50,000	6	5

histogram is for η sidebands ($0.45 \text{ GeV}/c^2 < m_{\gamma\gamma} < 0.50 \text{ GeV}/c^2$ and $0.60 \text{ GeV}/c^2 < m_{\gamma\gamma} < 0.65 \text{ GeV}/c^2$). From Fig. 2, we conclude that the K_S^0 signals are consistent with coming from background, as estimated from η sideband events.

The $m_{\gamma\gamma}$ distribution, shown in Fig. 1, is fitted with a Monte Carlo determined shape for the η and a second order polynomial and yields 4839 ± 158 $J/\psi \rightarrow 2(\pi^+\pi^-)\eta$, $\eta \rightarrow \gamma\gamma$ events.

3 Analysis of $J/\psi \rightarrow 3(\pi^+\pi^-)\eta$

Events with six good charged tracks and at least two isolated photons are selected. The angle between two oppositely charged tracks is required to be greater than 10° to remove γ conversions. A four constraint kinematic fit is made to the hypothesis $J/\psi \rightarrow 3(\pi^+\pi^-)\gamma\gamma$, and $\chi^2_{\pi^+\pi^-\pi^+\pi^-\pi^+\pi^-\gamma\gamma}$ is required to be less than 15.

After the above selection, the two photon invariant mass distribution is shown in Fig. 3; an η signal is evident.

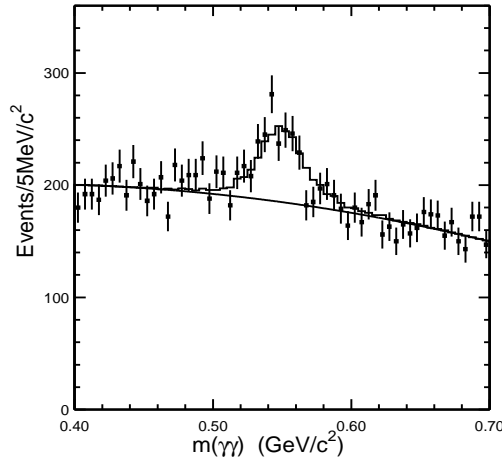


Fig. 3. Distribution of $m_{\gamma\gamma}$ for $J/\psi \rightarrow 3(\pi^+\pi^-)\gamma\gamma$ candidate events. Dots with error bars are data, the histogram is the η shape determined by Monte Carlo simulation, and the curve is background.

Monte Carlo simulation indicates that background from the decay modes listed in Table 1 can be ignored. Other possible backgrounds are from $J/\psi \rightarrow \gamma 2(\pi^+\pi^-)\eta$ and $J/\psi \rightarrow \gamma 3(\pi^+\pi^-)\eta$ events. As described in Section 2, the $m_{\gamma\gamma}$ distribution from $J/\psi \rightarrow \gamma 2(\pi^+\pi^-)\eta$ shows no clear η peak. For $J/\psi \rightarrow \gamma 3(\pi^+\pi^-)\eta$, the $m_{\gamma\gamma}$ distribution from Monte Carlo simulation, shown in Fig. 4(a), also does not show a peak in the η region, so its contribution can also be ignored.

The background with K_S^0 final states can also be estimated, as was done previously, using the η sidebands. Fig. 4(b) shows the $\pi^+\pi^-$ mass distribution. The full histogram is the $m_{\pi^+\pi^-}$ distribution for events in the η signal region ($|m_{\gamma\gamma} - 0.55| < 0.05 \text{ GeV}/c^2$), and the shaded histogram is for events from the

η sidebands ($0.45 \text{ GeV}/c^2 < m_{\gamma\gamma} < 0.50 \text{ GeV}/c^2$ and $0.60 \text{ GeV}/c^2 < m_{\gamma\gamma} < 0.65 \text{ GeV}/c^2$). As in Section 2, we can conclude from Fig. 4(b) that most events with K_S^0 are associated with backgrounds which are measured by η sidebands.

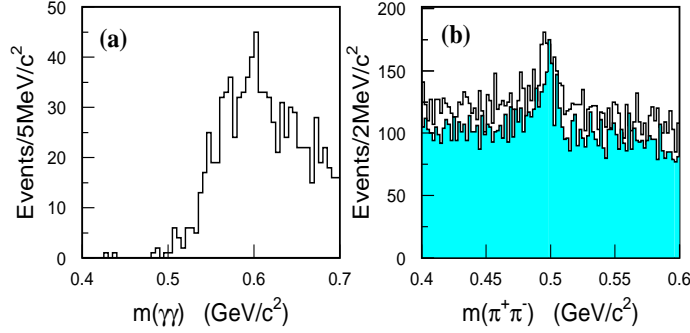


Fig. 4. (a) The $m_{\gamma\gamma}$ distribution from Monte Carlo simulation of $J/\psi \rightarrow \gamma 3(\pi^+\pi^-)\eta$; (b) The distribution of $m_{\pi^+\pi^-}$ from η signal events (histogram) and η sidebands (shaded histogram) for $J/\psi \rightarrow \gamma\gamma 3(\pi^+\pi^-)$ events.

Fitting the $\gamma\gamma$ mass distribution in Fig. 3 with the Monte Carlo shape for η and a second order polynomial, as described in Section 2, yields 616 ± 82 events.

4 Detection efficiency

Initially events were generated according to uniform phase space. However, the $\cos\theta$ distribution of charged tracks in $J/\psi \rightarrow 2(\pi^+\pi^-)\eta$ was inconsistent with that from Monte Carlo simulation. Much better agreement is obtained when the angular distribution is generated according to $1 + \alpha \cos^2\theta$, where $\alpha = 0.65 \pm 0.03$ is obtained by fitting the $\cos\theta$ distribution of charged tracks. Fig. 5(a) and Fig. 5(b) show the comparison of the $\cos\theta$ distributions for charged tracks and η , respectively, with Monte Carlo simulated events with the charged tracks generated according to this distribution. Including the contribution from η sidebands, the angular distributions are consistent.

For $J/\psi \rightarrow 3(\pi^+\pi^-)\eta$, the detection efficiency is obtained from phase space events since the $\cos\theta$ distributions of charged tracks and η are consistent with those from Monte Carlo simulation, as shown in Fig. 6(a) and Fig. 6(b), respectively. For the above two decay modes, the detection efficiencies are listed in Table 3.

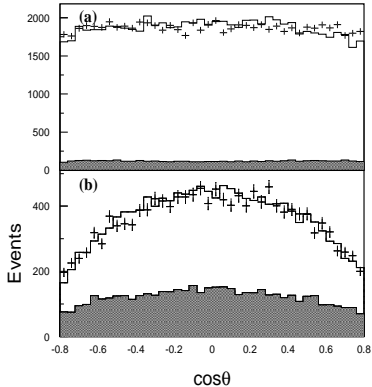


Fig. 5. The $\cos\theta$ distribution of (a) charged tracks and (b) η particles, where the crosses are data, the shaded histogram is from Monte Carlo simulation of $J/\psi \rightarrow 2(\pi^+\pi^-\eta)$, and the full histogram is the sum of sideband background and Monte Carlo simulation.

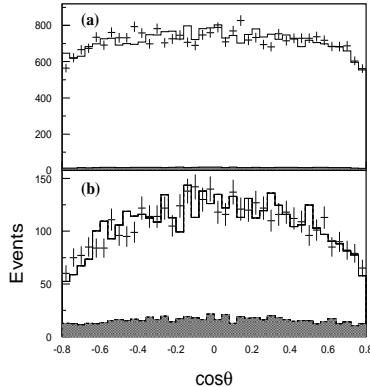


Fig. 6. The $\cos\theta$ distribution of (a) charged tracks and (b) η particles, where the crosses are data, the shaded histogram is from Monte Carlo simulation of $J/\psi \rightarrow 3(\pi^+\pi^-\eta)$, and the full histogram is the sum of sideband background and Monte Carlo simulation.

5 Systematic errors

The systematic errors mainly come from the following sources:

(1) The MDC tracking efficiency has been measured using channels like $J/\psi \rightarrow \Lambda\bar{\Lambda}$ and $\psi(2S) \rightarrow \pi^+\pi^-J/\psi$, $J/\psi \rightarrow \mu^+\mu^-$. It is found that the Monte Carlo simulation agrees with data within 1-2% for each charged track. Therefore, 8% and 12% are taken as the systematic errors in the tracking efficiencies for the 4-prong and 6-prong final states analyzed here.

(2) The photon detection efficiency has been studied with different methods using $J/\psi \rightarrow \rho^0\pi^0$ events [7]; the difference between data and Monte Carlo simulation is about 2% for each photon. In this analysis, 4% is taken as the systematic error for the η decaying into two photons.

(3) The kinematic fit is useful to reduce background. The systematic error from the kinematic fit is studied using the clean channel $J/\psi \rightarrow \pi^+\pi^-\pi^0$, as described in Ref. [5]. The efficiency difference of the kinematic fit between data and Monte Carlo simulation is about 4%. With the same method, the decay modes $J/\psi \rightarrow 2(\pi^+\pi^-\pi^0)$ and $J/\psi \rightarrow 3(\pi^+\pi^-\pi^0)$ are also analyzed. The efficiency difference of kinematic fit between data and Monte Carlo are 4.3% and 5.5% respectively. Since $J/\psi \rightarrow 2(\pi^+\pi^-\pi^0)$ and $J/\psi \rightarrow 3(\pi^+\pi^-\pi^0)$

are similar to the two channels analyzed in this paper, 4.3% and 5.5% are taken as the systematic error of the kinematic fit.

(4) Other possible J/ψ decay modes which may contribute to η signals have been studied, and the background from them can be ignored. The error from the background under the η peak is included in the fitting error. The uncertainties of the background shape in the two channels are estimated to be about 3.4% by changing the order of the polynomial. Possible background from the continuum events [8] is estimated using data at $\sqrt{s} = 3.07$ GeV/c. After applying the same selection criteria as above, no significant η signal is observed. Therefore, the background from this source is also negligible. From the above analysis, the background uncertainty for the two decay modes is less than 5%, which is taken as the background systematic error.

(5) The branching fraction of $\eta \rightarrow \gamma\gamma$ is $(39.43 \pm 0.26)\%$ [6]. The error is also taken as a systematic error.

(6) The number of J/ψ events is $(57.70 \pm 2.72) \times 10^6$, determined from inclusive 4-prong hadrons [9]. The uncertainty, 4.7%, is also a systematic error. Table 2 lists the systematic errors from all sources.

Table 2

Summary of systematic errors (%)

Source	$2(\pi^+\pi^-\eta)$	$3(\pi^+\pi^-\eta)$
MDC Tracking	8	12
Photon efficiency	4	4
Kinematic fit	4.3	5.5
Background	5	5
$B(\eta \rightarrow \gamma\gamma)$	0.7	0.7
Number of J/ψ events	4.7	4.7
Total	12.1	15.4

6 Results

The branching fractions are calculated with the following relation:

$$B(J/\psi \rightarrow n(\pi^+\pi^-\eta)) = \frac{N_{obs}}{\varepsilon \cdot B(\eta \rightarrow \gamma\gamma) \cdot N_{J/\psi}}, \quad (1)$$

where n is 2 or 3, N_{obs} is the observed events, ε is the detection efficiency, $B(\eta \rightarrow \gamma\gamma)$ is the branching fraction of $\eta \rightarrow \gamma\gamma$, and $N_{J/\psi}$ the total number

of J/ψ events.

Table 3 summarizes the quantities used in the calculation of the two branching fractions and the final results, including systematic errors.

Table 3

Numbers used and branching fractions measured.

Decay Modes	N_{obs}	$\varepsilon(\%)$	Branching Fraction
$J/\psi \rightarrow 2(\pi^+\pi^-)\eta$	4839 ± 158	9.43 ± 0.10	$(2.26 \pm 0.08 \pm 0.27) \times 10^{-3}$
$J/\psi \rightarrow 3(\pi^+\pi^-)\eta$	616 ± 82	3.74 ± 0.06	$(7.24 \pm 0.96 \pm 1.11) \times 10^{-4}$

7 Summary

In this paper, the decays of $J/\psi \rightarrow 2(\pi^+\pi^-)\eta$ and $J/\psi \rightarrow 3(\pi^+\pi^-)\eta$ are studied with the BESII 5.8×10^7 J/ψ event sample and their branching fractions are measured for the first time to be:

$$B(J/\psi \rightarrow 2(\pi^+\pi^-)\eta) = (2.26 \pm 0.08 \pm 0.27) \times 10^{-3}$$

$$B(J/\psi \rightarrow 3(\pi^+\pi^-)\eta) = (7.24 \pm 0.96 \pm 1.11) \times 10^{-4}$$

Comparing with other branching fractions of J/ψ decaying into stable hadrons, the branching fractions of $J/\psi \rightarrow 2(\pi^+\pi^-)\eta$ and $J/\psi \rightarrow 3(\pi^+\pi^-)\eta$ are not large.

The BES collaboration thanks the staff of BEPC and the computing center for their hard efforts. This work is supported in part by the National Natural Science Foundation of China under contracts Nos. 19991480, 10225524, 10225525, the Chinese Academy of Sciences under contract No. KJ 95T-03, the 100 Talents Program of CAS under Contract Nos. U-11, U-24, U-25, and the Knowledge Innovation Project of CAS under Contract Nos. U-602, U-34 (IHEP); and by the National Natural Science Foundation of China under Contract No.10175060 (USTC), and No. 10225522 (Tsinghua University); and by the U. S. Department of Energy under Contract N0. DE-FG02-04ER41291.

References

- [1] J. J. Aubert, et al., Phys. Rev. Lett. 33 (1974) 1404.
- [2] J. E. Augustin, et al., Phys. Rev. Lett. 33 (1974) 1406.
- [3] L. Kopke and A. Wermes, Phys. Rep. 174 (1989) 67.

- [4] J. Z. Bai, et al., Nucl. Instrum. Methods, A458 (2001) 627.
- [5] J. Z. Bai, et al., Phys. Rev. D70 (2004) 012005.
- [6] S. Eidelman, et al.,(Particle Data Group), Phys. Lett. B592 (2004) 1, and references therein.
- [7] S. M. Li, et al., High Energy Phys. and Nucl. Phys. 28 (2004) 859 (in Chinese).
- [8] P. Wang, X. H. Mo, C. Z. Yuan, Phys. Lett. B557 (2003) 192
- [9] S. S. Fang, et al., High Energy Phys. and Nucl. Phys. 27,(2003) 277 (in Chinese).